Commun. Comput. Phys.
doi: 10.4208/cicp.171114.140715a

Vol. **19**, No. 1, pp. 24-52
January 2016

Geometric Numerical Integration for Peakon b-Family Equations

Wenjun Cai[1,3], Yajuan Sun[2,*] and Yushun Wang[3]

[1] *Key Laboratory of Computational Geodynamics, University of Chinese Academy of Sciences, Beijing 100049, China.*
[2] *LSEC, Academy of Mathematics and Systems Science, Chinese Academy of Sciences, Beijing 100190, China.*
[3] *Jiangsu Provincial Key Laboratory for NSLSCS, School of Mathematical Sciences, Nanjing Normal University Nanjing 210023, China.*

Received 17 November 2014; Accepted (in revised version) 14 July 2015

Abstract. In this paper, we study the Camassa-Holm equation and the Degasperis-Procesi equation. The two equations are in the family of integrable peakon equations, and both have very rich geometric properties. Based on these geometric structures, we construct the geometric numerical integrators for simulating their soliton solutions. The Camassa-Holm equation and the Degasperis-Procesi equation have many common properties, however they also have the significant difference, for example there exist the shock wave solutions for the Degasperis-Procesi equation. By using the symplectic Fourier pseudo-spectral integrator, we simulate the peakon solutions of the two equations. To illustrate the smooth solitons and shock wave solutions of the DP equation, we use the splitting technique and combine the composition methods. In the numerical experiments, comparisons of these two kinds of methods are presented in terms of accuracy, computational cost and invariants preservation.

AMS subject classifications: 35L65, 65M70, 65N06, 65P10, 74J40

Key words: Symplectic integrator, splitting method, WENO scheme, multisymplectic integrator, peakon, shockpeakon.

1 Introduction

In the soliton theory, it is important to study the completely integrable nonlinear partial differential equations which arise from approximating the shallow water systems. Such equations usually have infinite number of conservation laws, and admit the soliton solutions which have the localized spatial structures and show the particle-like scattering

*Corresponding author. *Email addresses:* wenjuncai1@gmail.com (W. Cai), sunyj@lsec.cc.ac.cn (Y. Sun), wangyushun@njnu.edu.cn (Y. Wang)

behavior. In this paper, our interest is to study a family of third-order dispersive nonlinear equations

$$u_t+c_0u_x-u_{xxt}+(\beta+1)uu_x-\beta u_xu_{xx}-uu_{xxx}=0, \tag{1.1}$$

where β is a bifurcation or balance parameter which provides a balance for the behavior of nonlinear solutions, and uu_x refers to the advection term which coefficient $\beta+1$ often causes a steepening of wave. The family of PDEs (1.1) includes two important equations: the Camassa-Holm (CH) equation (when $\beta=2,c_0=2\kappa^2$) [5] and the Degasperis-Procesi (DP) equation (when $\beta=3,c_0=3\kappa^3$) [14]. Both the CH equation and the DP equation can be viewed as the model equations of shallow water waves [5,6,12,22]. By presenting the Lax pair and bi-Hamiltonian structure, it has been proved that the two systems are completely integrable [6,13]. In the absence of linear dispersion term u_{xxx}, with the nonlinear dispersion term uu_{xxx} the DP and CH equations have the novel properties one of which is that they admit the peakon soliton solutions [5, 13, 14]. To derive the peakon soliton solutions exactly, we can use the inverse scattering techniques [1,2,28,29].

Although the CH and the DP equations have shared some common properties, they are divergent by having the major differences: Lax pair equation and wave breaking phenomena [13,27]. The isospectral problem in Lax pair for the DP equation is the third-order equation while one is the second-order equation for the CH equation. Thus, the DP equation has more types of solutions than the CH equation. It is illustrated in [9,27] that the DP equation has not only the peakon solutions, but also the shockpeakon solutions which produce the difficulty to capture the shock wave numerically. Compared with the CH equation, there exist only few numerical methods and corresponding numerical analysis for the DP equation. The existing numerical methods for the DP equation include the operator splitting schemes [8], the particle method based on the multi-shockpeakon solutions [20], the conservative finite difference schemes [32], local discontinuous Galerkin (LDG) methods [41], the direct discontinuous Galerkin (DDG) method [25], the compact finite difference method [44] and the spectral method [40], etc.

As a class of conservative PDEs, the DP and CH equations have many conservative properties, such as the bi-Hamiltonian structures, infinite number of conservation laws etc. A natural idea of numerical computation for the two systems is to construct the numerical methods which can carry as much as possible these intrinsic properties. Geometric numerical integrators are a kind of numerical methods constructed based on this idea [19]. Compared with the non-geometric numerical integrators, geometric numerical integrators usually illustrate the remarkable capacity to capture the dynamical behavior of the given system over long time [19]. Based on Hamiltonian structure of the DP and CH equations, our purpose of this paper is to construct the corresponding numerical methods. To simulate the peakon solutions of the two equations, we present the numerical discretization which is given by using the pseudo-spectral method in space and symplectic integrator in time. By means of fast Fourier transform (FFT), the numerical solution with exponential convergency can be obtained if the solution is smooth enough. The numerical results show the long-term stability of the symplectic pseudo-

spectral method in simulating the peakon solutions, and also the good performance in preserving the invariants. To simulate the shockpeakon wave of the DP equation, we use the splitting technique presented in [8,16]. The DP equation can be decomposed as the Benjamin-Bona-Mahony (BBM) equation and the Burgers' equation. By composing the multisymplectic method for the BBM equation and the WENO method of fifth-order for the Burgers' equation, we obtain the spatial semi-discretization of the DP equation. The full discretization for the DP equation is obtained by using the splitting method of higher-order in time.

This paper is organized as follows. In Section 2, two symplectic pseudo-spectral integrators are proposed based on Hamiltonian formulations of the CH and DP equations. In Section 3, the DP equation is split as a composition of conservative system (BBM equation) and hyperbolic system (Burgers' equation). The multisymplectic pseudo-spectral method is applied to the BBM equation while the WENO method of fifth-order is applied to the Burger's equation. The full discretization is presented when the composition method is applied in space and temporal discretization is also used. Section 4 is devoted to numerical experiments in which we simulate the soliton solution, the peakon solution, and also the shockpeakon solution. The numerical errors of solutions and conservative quantities are also presented in this section. We conclude this paper in Section 5.

2 Symplectic Fourier pseudo-spectral integrator for CH and DP equations

In this section, we present the symplectic Fourier pseudo-spectral integrators for the CH and DP equations based on their Hamiltonian formulations.

First, we introduce the Hamiltonian formulations of the two equations. In the family of PDEs (1.1), taking $\kappa=0$ gives the CH equation and the DP equation in the following form:

$$u_t-u_{xxt}+3uu_x-2u_xu_{xx}-uu_{xxx}=0 \tag{2.1}$$

and

$$u_t-u_{xxt}+4uu_x-3u_xu_{xx}-uu_{xxx}=0. \tag{2.2}$$

By denoting $m=(1-\partial_x^2)u$, (2.1) and (2.2) can be simplified to

$$m_t+um_x+2u_xm=0, \tag{2.3}$$
$$m_t+um_x+3u_xm=0, \tag{2.4}$$

where $u(x,t)$ can be solved by

$$u(x,t)=\frac{1}{2}\int_{-\infty}^{\infty}\exp(-|x-y|)m(y,t)dy$$

with Helmholtz operator $1-\partial_x^2$. Let $\mathcal{B}_0$, $\mathcal{B}_1$ and $\widehat{\mathcal{B}}_0$, $\widehat{\mathcal{B}}_1$ be operators given by

$$\mathcal{B}_0=\partial_x(1-\partial_x^2),\quad \mathcal{B}_1=\partial_x m\cdot+m\partial_x\cdot,$$
$$\widehat{\mathcal{B}}_0=\partial_x(1-\partial_x^2)(4-\partial_x^2),\quad \widehat{\mathcal{B}}_1=m^{\frac{2}{3}}\partial_x m^{\frac{1}{3}}\cdot(\partial_x-\partial_x^3)^{-1}m^{\frac{1}{3}}\partial_x m^{\frac{2}{3}}\cdot,$$

where $\partial_x m\cdot v:=(mv)_x$. Then, the CH and DP equations can be written as [6, 13]

$$m_t=\mathcal{B}_0\frac{\delta\mathcal{H}_0}{\delta m}=\mathcal{B}_1\frac{\delta\mathcal{H}_1}{\delta m}, \tag{2.5}$$
$$m_t=\widehat{\mathcal{B}}_0\frac{\delta\widehat{\mathcal{H}}_0}{\delta m}=\widehat{\mathcal{B}}_1\frac{\delta\widehat{\mathcal{H}}_1}{\delta m}, \tag{2.6}$$

where

$$\mathcal{H}_0=-\frac{1}{2}\int_{-\infty}^{\infty}(u^3+uu_x^2)dx,\quad \mathcal{H}_1=-\frac{1}{2}\int_{-\infty}^{\infty}(u^2+u_x^2)dx, \tag{2.7a}$$
$$\widehat{\mathcal{H}}_0=-\frac{1}{6}\int_{-\infty}^{\infty}u^3dx,\quad \widehat{\mathcal{H}}_1=-\frac{9}{2}\int_{-\infty}^{\infty}mdx. \tag{2.7b}$$

The two forms (2.5) and (2.6) are both infinite dimensional Hamiltonian systems with bi-Hamiltonian structures since $\mathcal{B}_0$, $\mathcal{B}_1$ and $\widehat{\mathcal{B}}_0$, $\widehat{\mathcal{B}}_1$ can be proved to be the Hamiltonian operators[†]. Notice $\partial_x m\cdot v:=(mv)_x$, then $\mathcal{B}_1$ and $\widehat{\mathcal{B}}_1$ can be calculated as

$$\mathcal{B}_1 v=m_x v+2mv_x,$$
$$\widehat{\mathcal{B}}_1 v=\frac{1}{3}m_x(\partial_x-\partial_x^3)^{-1}\Big(\frac{2}{3}m_x v+mv_x\Big)+m(1-\partial_x^2)^{-1}\Big(\frac{2}{3}m_x v+mv_x\Big).$$

Denote the functional derivative[‡] by $\frac{\delta\mathcal{H}}{\delta m}$, using its definition gives

$$\frac{\delta\mathcal{H}_0}{\delta m}=(1-\partial_x^2)^{-1}\Big(-\frac{3}{2}u^2+\frac{1}{2}u_x^2+uu_{xx}\Big),\quad \frac{\delta\mathcal{H}_1}{\delta m}=-u,$$
$$\frac{\delta\widehat{\mathcal{H}}_0}{\delta m}=-\frac{1}{2}(1-\partial_x^2)^{-1}u^2,\quad \frac{\delta\widehat{\mathcal{H}}_1}{\delta m}=-\frac{9}{2}.$$

The formulations (2.5) and (2.6) can be derived following the above calculations. Furthermore, we can rewrite the formulations of the first kind for the CH and DP equations in terms of u as

$$u_t=(1-\partial_x^2)^{-1}\partial_x\frac{\delta\mathcal{H}_0}{\delta u} \tag{2.8}$$

and

$$u_t=(1-\partial_x^2)^{-1}\partial_x(4-\partial_x^2)\frac{\delta\widehat{\mathcal{H}}_0}{\delta u} \tag{2.9}$$

[†]A linear operator $\mathcal{D}$ which may depend on u and its higher-order derivatives, is called Hamiltonian if it satisfies $\{\mathcal{F},\mathcal{G}\}=-\{\mathcal{G},\mathcal{F}\}$ (skew-adjoint) and $\{\mathcal{R},\{\mathcal{F},\mathcal{G}\}\}+\{\mathcal{G},\{\mathcal{R},\mathcal{F}\}\}+\{\mathcal{F},\{\mathcal{G},\mathcal{R}\}\}=0$ (Jacobi identity) for all functionals $\mathcal{F},\mathcal{G},\mathcal{R}$ of u. Here, $\{\cdot,\cdot\}$ denotes the Poisson bracket defined by $\{\mathcal{F},\mathcal{G}\}=\int_{-\infty}^{\infty}\frac{\delta\mathcal{F}}{\delta u}\mathcal{D}\frac{\delta\mathcal{G}}{\delta u}dx$.
[‡]The functional derivative $\frac{\partial\mathcal{H}}{\partial m}$ is defined by $\int_{-\infty}^{\infty}\frac{\delta\mathcal{H}}{\delta m}\delta m dx=\lim_{\tau\to0}(\mathcal{H}(m+\tau\delta m)-\mathcal{H}(m))/\tau$.

which are Hamiltonian. In the following discussion, we use the method of lines approach to construct the symplectic Fourier pseudo-spectral methods for the two equations based on their Hamiltonian formulations (2.8) and (2.9).

The method of lines approach is a technique which needs first to discretize the spatial derivatives and then to discretize the semi-discretized system by the corresponding ODEs solver, it is very often used in solving the PDEs. To get the spatial discretizations, we can use the Fourier spectral method which is obtained by approximating the unknown function with the finite sum of a series of trigonometric functions. The Fourier spectral method is very suitable for simulating the evolution of solutions in PDEs with periodic phenomena (refer to [34] for detail), and often refers to the Fourier pseudo-spectral method if requiring the approximate solution to satisfy the concerned equations at a set of collocation points. For Eqs. (2.8) and (2.9), we apply the Fourier pseudo-spectral method to obtain the semi-discretization of the CH and DP equations. In the semi-discretized system, the differential operator in PDEs is approximated by the so-called spectral differentiation matrix which computation can use the fast Fourier transform (FFT). The FFT algorithm plays an important role in the implementation of spectral method and can be used to get the numerical solution with a convergency of infinite order [39].

Suppose that the problem is defined on domain $\mathbf{R}^+\times[-L,L]$ with periodic boundary conditions. Take $x_j=-L+hj$, $0\le j\le N-1$ be the spatial grids with $h=2L/N$ the space step. The spectral method is to find an approximate solution in the form of

$$u(x,t)\approx\sum_{j=0}^{N-1}u_j\varphi_j(x):=I_Nu(x,t),$$

where $u_j=u(x_j,t)$, $\varphi_j(x)=\frac{1}{N}\sum_{k=-\frac{N}{2}}^{\frac{N}{2}-1}\exp(-ik\pi(x_j-x)/L)$. Notice $\varphi_j(x_j)=1$, $\varphi_j(x_l)=0$ for $l\neq j$, then

$$I_Nu(x_j,t)=u(x_j,t).$$

Define a map $F_N:I_Nu(x,t)\to U(t)=(u_0,\cdots,u_{N-1})$, then $F_NI_Nu(x,t)=I_Nu(x_j,t)$. Taking the m-th derivative ($m\ge1$) of $I_Nu(x,t)$ gives that

$$\frac{\partial^mI_Nu}{\partial x^m}(x_j,t)=\sum_{k=0}^{N-1}(D_m)_{j,k}u_k,$$

where D_m is called the m-differentiation matrices, for $m=1$ and 2 which are

$$(D_1)_{j,l}=\begin{cases}\frac{1}{2}\mu(-1)^{j+l}\cot\left(\mu\frac{x_j-x_l}{2}\right), & j\neq l,\\ 0, & j=l,\end{cases}\tag{2.10}$$

$$(D_2)_{j,l}=\begin{cases}\frac{1}{2}\mu^2(-1)^{j+l+1}\frac{1}{\sin^2(\mu(x_j-x_l)/2)}, & j\neq l,\\ -\mu^2\frac{2(N/2)^2+1}{6}, & j=l,\end{cases}\tag{2.11}$$

with $\mu=\frac{\pi}{L}$. Clearly, D_1 is skew-symmetric and D_2 is symmetric. For the Fourier pseudo-spectral method, the approximate solution $I_Nu(x,t)$ is required to satisfy the given PDEs at $\{x_j\}_{j=0}^{N-1}$. If the system of PDEs has a form of $\dot{u}=\mathcal{D}(u)\frac{\delta\mathcal{H}}{\delta u}$, then applying the Fourier pseudo-spectral method to it gives the following semi-discretized system

$$\frac{d}{dt}U=D(U)\nabla H(U), \tag{2.12}$$

where $D(U)V=F_N\circ I_N\circ\mathcal{D}(I_Nu)\circ F_N^{-1}(V)$, $H(U)=\int_{-L}^{L}\mathcal{H}(F_N^{-1}(U))dx$. It is shown that $D(U)$ is a $N\times N$ skew-symmetric matrix operator. In fact, it can be checked easily by

$$\begin{aligned}\big\langle D(U)V,W\big\rangle&=\big\langle F_N\circ I_N\circ\mathcal{D}(I_Nu)\circ F_N^{-1}(V),W\big\rangle_N\\&=\big\langle F_N^{-1}(V),\mathcal{D}(I_Nu)I_Nw\big\rangle\\&=\big\langle I_Nv,I_N\circ\mathcal{D}(I_Nu)I_Nw\big\rangle\\&=-\big\langle V,D(U)W\big\rangle_N,\end{aligned}$$

where $\langle\cdot,\cdot\rangle_N$ denotes the inner product in $\mathbf{R}^N$, $\langle\cdot,\cdot\rangle$ denotes the inner product in the function space. Specifically, the semi-discretized systems of the DP and CH equations by applying the Fourier pseudo-spectral method to (2.8) and (2.9) are

$$U_t=(I-D_2)^{-1}D_1\nabla H_0(U) \tag{2.13}$$

and

$$U_t=((I-D_2)^{-1}D_1(4-D_2)\nabla\widehat{H}_0(U), \tag{2.14}$$

where $H_0(U)=-\frac{1}{2}\sum_{j=0}^{N-1}\left(u_j^3+u_j((D_1U)_j)^2\right)$ and $\widehat{H}_0(U)=-\frac{1}{6}\sum_{j=0}^{N-1}u_j^3$ are two discrete Hamiltonians with D_1 and D_2 defined above.

Applying the symplectic midpoint point method to the semi-discretized systems (2.13) and (2.14), provides the full discretizations of the CH and DP equations which are denoted by **SFP-CH** and **SFP-DP**, respectively.

3 Operator splitting method for DP equation

The DP equation admits not only the peakon solution $u(x,t)=ce^{|x-ct|}$, but also the shock peakon solutions [27] (the entropy solutions [9]) of the form

$$u(x,t)=ce^{-|x-ct|}+\mathrm{sgn}(x-ct)\frac{s}{1+ts}e^{-|x-ct|}, \tag{3.1}$$

where $c,s(s>0)$ are two constants. The peakon and shock peakon solutions of the DP equation are not the strong solutions in the Sobolev space $H^s(s\geq\frac{3}{2})$, they are the global weak solutions in H^1 [15]. As the existence of these discontinuous solutions (shock waves [27]), the DP equation can show the completely different behaviour compared with the

CH equation. It has been confirmed by Coclite and Karlsen [9, 10] that the DP equation has the solution behaviour similar to ones of inviscid Burgers equation.

Consider the general DP equation

$$u_t+3\kappa^3u_x-u_{xxt}+4uu_x-3u_xu_{xx}-uu_{xxx}=0,\quad \kappa\neq 0. \tag{3.2}$$

To simulate the smooth soliton and shock peakon solutions of the DP equation (3.2), we construct the numerical methods based on operator splitting in this section. At the starting point, we reform the DP equation (3.2) in the hyperbolic-elliptic formulation

$$u_t+f(u)_x+P_x=0, \tag{3.3a}$$
$$(1-\partial_x^2)P=3\kappa^3u+3f(u), \tag{3.3b}$$

with $f(u)=\frac{1}{2}u^2$, which is used to define the weak solutions of the DP equation [8]. Splitting the first equation of (3.3) gives [8, 16]:

$$u_t+f(u)_x=0, \tag{3.4}$$
$$u_t+P_x=0. \tag{3.5}$$

Combine with the second equation of (3.3), it is observed that (3.5) is called the Benjamin-Bona-Mahhony (BBM) equation while (3.4) is the Burgers' equation. Using the operator technique, we can present the numerical methods for the DP equation by combing the classical numerical methods of the BBM equation and the Burgers' equation. To be self-contained, as follows we briefly introduce the numerical methods of the BBM equation and the Burgers' equation, respectively.

First, we consider the numerical methods for the Burgers' equation. The Burgers' equation is a model PDEs in fluid dynamics which usually admit the shock wave solution even the initial value is smooth. To capture the shock wave, the schemes are required to have the high-resolution with which the examples include the high-order total variation diminishing (TVD) schemes proposed firstly by Harten, the essentially non-oscillatory (ENO) schemes and the weighted essentially non-oscillatory (WENO) scheme etc. (refer to [21,35] and references therein). Due to its high order accuracy, fast implementation and smoother flux, we here take the WENO method of fifth-order to discretize the Burgers' equation (3.4) which leads to the following conservative form

$$\frac{\mathrm{d}u_j(t)}{\mathrm{d}t}=-\frac{1}{\Delta x}\left(\hat{f}_{j+\frac{1}{2}}-\hat{f}_{j-\frac{1}{2}}\right),\quad j=0,\cdots,N-1, \tag{3.6}$$

where Δx is the space step, $u_j\approx u(j\Delta x,t)$, $\hat{f}_{j-\frac{1}{2}}$ and $\hat{f}_{j+\frac{1}{2}}$ are called the numerical fluxes which can have various choices according to the given problems. In order to gain the numerical methods satisfying the monotone condition, the nonlinear term $f(u)$ usually needs to be split. For example, using the Lax-Friedrichs splitting gives

$$f(u)=f^+(u)+f^-(u),$$

where $f^{\pm}(u)=\frac{1}{2}(f(u)\pm\alpha u)$ with α the maximum of $|f'(u)|$ over the relevant range of u. It is clear that $\frac{\mathrm{d}f^{+}(u)}{\mathrm{d}u}\geq 0$ and $\frac{\mathrm{d}f^{-}(u)}{\mathrm{d}u}\leq 0$.

To define the numerical fluxes $\hat{f}_{j+\frac{1}{2}}$ and $\hat{f}_{j-\frac{1}{2}}$ for the fifth-order WENO scheme (3.6), we first denote $\bar{v}_j=f^{+}(u_j)$ and $V_j=[\bar{v}_j,\bar{v}_{j+1},\bar{v}_{j+2}]^T$. Let

$$\bar{v}^{(0)}_{j+\frac{1}{2}}=\alpha V_j,\quad \bar{v}^{(1)}_{j+\frac{1}{2}}=\beta V_{j-1},\quad \bar{v}^{(2)}_{j+\frac{1}{2}}=\gamma V_{j-2},$$

with $\alpha=[1/3,5/6,-1/6]$, $\beta=[-1/6,5/6,1/3]$, $\gamma=[1/3,-7/6,11/6]$. Take

$$\bar{v}^{-}_{j+\frac{1}{2}}=\omega_0\bar{v}^{(0)}_{j+\frac{1}{2}}+\omega_1\bar{v}^{(1)}_{j+\frac{1}{2}}+\omega_2\bar{v}^{(2)}_{j+\frac{1}{2}},$$

where ω_i are the nonlinear weights given by

$$\omega_j=\frac{\alpha_j}{\alpha_0+\alpha_1+\alpha_2},\quad \alpha_j=\frac{d_i}{(\epsilon+\beta_j)^2},\quad j=0,1,2,$$

with $d_0=3/10,d_1=3/5,d_2=1/10$, and the smoothness indicators

$$\begin{aligned}\beta_0&=13(a_1V_j)^2/12+(b_1V_j)^2/4,\\ \beta_1&=13(a_1V_{j-1})^2/12+(b_2V_{j-1})^2/4,\\ \beta_2&=13(a_1V_{j-2})^2/12+(b_3V_{j-2})^2/4.\end{aligned}$$

Here, $a_1=[1,-2,1]$, $b_1=[3,-4,1]$, $b_2=[1,0,-1]$, $b_3=[1,-4,3]$ are the three-dimensional vectors, ϵ is a parameter which often is chosen as $\epsilon=10^{-6}$. The fifth-order WENO scheme is derived by taking the numerical fluxes as

$$\hat{f}_{j+\frac{1}{2}}=\hat{f}^{+}_{j+\frac{1}{2}}+\hat{f}^{-}_{j+\frac{1}{2}},\quad \hat{f}_{j-\frac{1}{2}}=\hat{f}^{+}_{j-\frac{1}{2}}+\hat{f}^{-}_{j-\frac{1}{2}},\tag{3.7}$$

where $\hat{f}^{+}_{j+\frac{1}{2}}=\bar{v}^{-}_{j+\frac{1}{2}}$ is called the positive flux which can turn into the negative flux $\hat{f}^{-}_{j+\frac{1}{2}}$ while a mirror image with respect to $j+\frac{1}{2}$ is applied.

For the semi-discretized system obtained by applying the fifth-order WENO scheme to the Burgers' equation, we use the so-called TVD Runge-Kutta method [36,37] in time. A third-order TVD Runge-Kutta method applied to $u_t=L(u)$ is

$$\begin{aligned}u^{(1)}&=u^n+\Delta tL(u^n),\\ u^{(2)}&=\frac{3}{4}u^n+\frac{1}{4}u^{(1)}+\frac{1}{4}\Delta tL(u^{(1)}),\\ u^{n+1}&=\frac{1}{3}u^n+\frac{2}{3}u^{(2)}+\frac{2}{3}\Delta tL(u^{(2)}),\end{aligned}$$

which can be described with the following Butcher tableau:

$$\begin{array}{c|ccc} 0 & 0 & 0 & 0 \\ 1 & 1 & 0 & 0 \\ \frac{1}{2} & \frac{1}{4} & \frac{1}{4} & 0 \\ \hline 1 & \frac{1}{6} & \frac{1}{6} & \frac{2}{3} \end{array}$$

The TVD Runge-Kutta method is a class of Runge-Kutta methods which was originally used in combination with the TVD scheme in space to solve the shock wave equation. It has the strong stability in any semi-norm (total variation norm, maximum norm, entropy condition, etc.), and is generalized further in [17,18].

Second, we consider the numerical methods of the regularized long-wave (RLW) equation (3.5). The RLW equation was first put forward by Peregrine (1966) to describe the development of long wave behaviour, then was named after T.B. Benjamin, J.L. Bona and J. Mahoney by P.J. Olver [33]. In [3], the details of existence, uniqueness and stability of the solutions of equation (3.5) had been studied. From the description of PDEs, the BBM equation is very similar to the KDV equation, but it diverges from the KdV equation by having only three conservation laws. Thus, the BBM equation is not integrable which can also be verified by that the solitary waves of the BBM equation show a non-elastic interaction.

The BBM equation is a conservative system which can be written as an infinite Hamiltonian system [33]

$$u_t = -(1-\partial_x^2)^{-1}\partial_x \frac{\delta \mathcal{H}}{\delta u}, \tag{3.8}$$

where $-(1-\partial_x^2)^{-1}\partial_x$ is the Hamiltonian operator and $\mathcal{H} = \frac{1}{6}\int_{-L}^{L} u^3 dx$ is the Hamiltonian functional. By introducing the bundle coordinates, the BBM equation (3.5) can also be written as a multisymplectic system which is [38]

$$Mz_t + Kz_x = \nabla_z S(z), \quad z \in \mathbb{R}^5, \tag{3.9}$$

with $z = (\psi, u, v, w, p)^T$, $S = up - \frac{3}{2}\kappa^3 u^2 - \frac{1}{2}u^3 + \frac{1}{2}vw$ and

$$M = \begin{bmatrix} 0 & -\frac{1}{2} & 0 & 0 & 0 \\ \frac{1}{2} & 0 & -\frac{1}{2} & 0 & 0 \\ 0 & \frac{1}{2} & 0 & 0 & 0 \\ 0 & 0 & 0 & 0 & 0 \\ 0 & 0 & 0 & 0 & 0 \end{bmatrix}, \quad K = \begin{bmatrix} 0 & 0 & 0 & 0 & -1 \\ 0 & 0 & 0 & -\frac{1}{2} & 0 \\ 0 & 0 & 0 & 0 & 0 \\ 0 & \frac{1}{2} & 0 & 0 & 0 \\ 1 & 0 & 0 & 0 & 0 \end{bmatrix}.$$

The multisymplectic conservation law for the BBM equation is

$$\frac{\partial}{\partial t}(\mathrm{d}u \wedge \mathrm{d}\psi + \mathrm{d}v \wedge \mathrm{d}u) + \frac{\partial}{\partial x}(2\mathrm{d}p \wedge \mathrm{d}\psi + \mathrm{d}w \wedge \mathrm{d}u) = 0.$$

Here, we apply the multisymplectic pseudo-spectral method [4, 7] to the BBM equation (3.9), it reads

$$M\frac{\mathrm{d}}{\mathrm{d}t}z_j+K\sum_{k=0}^{N-1}(D_1)_{j,k}z_k=\nabla_z S(z_j),\quad j=0,\cdots,N-1, \tag{3.10}$$

where $z_j=(\psi_j,u_j,v_j,w_j,p_j)^T$. By applying the implicit midpoint rule to the semi-discretized system (3.10), we derive the full discretization as follows:

$$M\delta_t^+ z_j^n+K\sum_{k=0}^{N-1}(D_1)_{j,k}z_k^{n+\frac{1}{2}}=\nabla_z S(z_j^{n+\frac{1}{2}}), \tag{3.11}$$

where δ_t^+ denotes the forward difference operator by $\delta_t^+ z_j^n=(z_j^{n+1}-z_j^n)/\Delta t$, and $z_j^{n+\frac{1}{2}}=(z_j^{n+1}+z_j^n)/2$. Scheme (3.11) is called multisymplectic as it preserves the following discrete multisymplectic conservation law

$$\frac{\omega_j^{n+1}-\omega_j^n}{\Delta t}+\sum_{k=0}^{N-1}(D_1)_{j,k}\kappa_{j,k}^{n+\frac{1}{2}}=0,\quad j=0,1,\cdots,N-1, \tag{3.12}$$

where $\omega_j^n=\mathrm{d}z_j^n\wedge M\mathrm{d}z_j^n$ and $\kappa_{j,k}^{n+\frac{1}{2}}=\mathrm{d}z_j^{n+\frac{1}{2}}\wedge K\mathrm{d}z_k^{n+\frac{1}{2}}$. As D_1 is skew-symmetric and $\kappa_{j,k}=\kappa_{k,j}$, taking the sum of (3.12) from $j=0$ to $N-1$ gives the global symplecticity which is shown as

$$\sum_{j=0}^{N-1}\frac{\omega_j^{n+1}-\omega_j^n}{\Delta t}=0.$$

To implement (3.11) practically, we obtain the following equivalent scheme by eliminating the medium variables from (3.11) that

$$\delta_t^+ U^n-\delta_t^+ D_1^2 U^n+D_1\Big(3\kappa^3 U^{n+\frac{1}{2}}+\frac{3}{2}(U^{n+\frac{1}{2}})^2\Big)=0, \tag{3.13}$$

where $U^n=(u_0^n,\cdots,u_{N-1}^n)^T$. After the above discretization, we denote the numerical solutions of the Burgers' equation and the BBM equation by $\varphi_{\Delta x,\Delta t}^{[1]}$ and $\varphi_{\Delta x,\Delta t}^{[2]}$, respectively. Via the general splitting technique [42, 43], the resulting numerical discretization of the DP equation can be derived by combining $\varphi_{\Delta x,\Delta t}^{[1]}$ and $\varphi_{\Delta x,\Delta t}^{[2]}$ as

$$\Psi_{\Delta x,\Delta t}=\varphi_{\Delta x,b_m\Delta t}^{[1]}\circ\varphi_{\Delta x,a_m\Delta t}^{[2]}\circ\cdots\circ\varphi_{\Delta x,b_1\Delta t}^{[2]}\circ\varphi_{\Delta x,a_1\Delta t}^{[1]}. \tag{3.14}$$

Taking the second-order Strang splitting method, i.e., $a_1=a_2=1/2, b_1=1, b_2=0$ in (3.14), we derive a full discretization for the DP equation (2.2) which is denoted by **OSM-DP**. Note that in time discretizations, although we have applied a third-order TVD Runge-Kutta method and a second-order midpoint rule for the Burgers' equation and the BBM equation respectively, the temporal accuracy of the final scheme **OSM-DP** is only second order due to the Strang splitting method. High-order method can be achieved by increasing the splitting stage in (3.14), which however will bring larger computational cost.

4 Numerical experiments

In the numerical experiments, we implement the numerical methods presented in the previous section. We simulate the peakon solutions for the CH equation by using scheme **SFP-CH** (2.13). We also simulate the peakon and shockpeakon waves for the DP equation by using schemes **SFP-DP** (2.14) and **OSM-DP** (3.14). For all the simulation, we employ the periodic boundary condition.

Denote $u_j^n \approx u(j\Delta x, n\Delta t)$ be the approximate solution at $(x=j\Delta x, t=n\Delta t)$. The numerical errors in L^1 and L^∞ norms are defined by

$$||e^n||_1 = \sum_{j=0}^{N-1} |u_j^n - u(j\Delta x, n\Delta t)|\Delta x, \quad ||e||_\infty = \max_{j=0,\cdots,N-1} |u_j^n - u(j\Delta x, n\Delta t)|.$$

It is known that the CH equation and the DP equation are completely integrable which states that they have the infinite number of conservation laws. Among these conservation laws, the three most important conserved quantities defined on $[-L,L]$ are

$$\mathcal{I}_0 = \int_{-L}^{L} (u^3 + uu_x^2)dx, \quad \mathcal{I}_1 = \int_{-L}^{L} (u^2 + u_x^2)dx, \quad \mathcal{I}_2 = \int_{-L}^{L} udx$$

for the CH equation (2.1) and

$$\widehat{\mathcal{I}}_0 = \int_{-L}^{L} u^3 dx, \quad \widehat{\mathcal{I}}_1 = \int_{-L}^{L} (u - u_{xx})dx, \quad \widehat{\mathcal{I}}_2 = \int_{-L}^{L} udx$$

for the DP equation (2.2). Accordingly, we define the discrete conserved invariants at time $t=n\Delta t$ as

$$I_0^n = \sum_{j=0}^{N-1} \left((u_j^n)^3 + u_j (D_1 U)_j^2\right)\Delta x, \quad I_1^n = \sum_{j=0}^{N-1} \left((u_j^n)^2 + (D_1 U^n)_j^2\right)\Delta x, \quad I_2^n = \sum_{j=0}^{N-1} u_j^n \Delta x,$$

and

$$\widehat{I}_0^n = \sum_{j=0}^{N-1} (u_j^n)^3 \Delta x, \quad \widehat{I}_1^n = \sum_{j=0}^{N-1} (u_j^n - (D_2 U^n)_j)\Delta x, \quad \widehat{I}_2^n = \sum_{j=0}^{N-1} u_j^n \Delta x,$$

where D_1, D_2 are the spectral differential matrices defined in (2.10), (2.11). The errors of three numerical invariants are calculated by $|I_i^n - I_i^0|$ and $|\widehat{I}_i^n - \widehat{I}_i^0|$ for $i=0,1,2$ respectively. Since I_2^n is linear invariant, it can be preserved by scheme **SFP-CH** to round-off errors. Similarly, **SFP-DP** can also preserve the invariants $\widehat{I}_1^n$ and $\widehat{I}_2^n$ exactly for the peakon solutions. However, for the discontinuous shockpeakon waves the continuous invariants $\widehat{\mathcal{I}}_0$ and $\widehat{\mathcal{I}}_1$ are no long conserved (see [27]), so are the discrete version of these two invariants.

As follows, we first present the numerical experiments for the CH equation (2.1) computed by **SFP-CH**.

Example 4.1. Smooth travelling wave solution for the CH equation

In this example, we consider a smooth travelling wave solution for the CH equation and test the accuracy of scheme **SFP-CH**. As pointed in [23, 24], the smooth periodic travelling wave can be described by three parameters $m,M,z\in\mathbb{R}$ with $z=c-M-m$ when the parameters satisfy the condition $z<m<M<c$. By choosing $m=0.3,M=0.7$ and $c=1$, following the procedures in [23], we can construct a smooth wave with period $a\approx 6.56$, see Fig. 1. The computing time is taken as $T=a/4$ and $\Delta t=0.0005\cdot T$. Table 1 presents the errors due to the spatial discretization which exhibit an exponentially convergence order in both the L_1 and L_∞ norms. Note however, that the error is limited with $N=64$ because the smooth travelling waves are not known in closed form. We also test the convergence order for the temporal discretization with fixed $N=256$ and $T=a$ in Table 2 which shows the second order of scheme **SFP-CH** because we have applied the implicit midpoint rule.

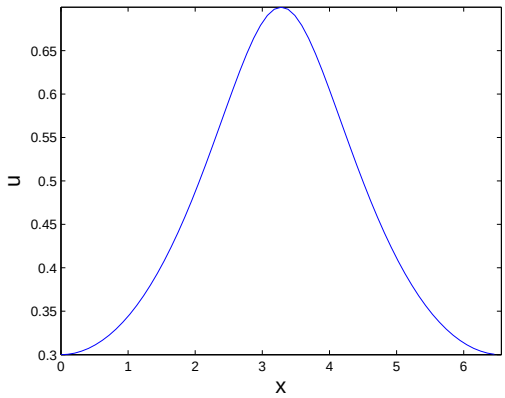

Figure 1: Initial profile of the smooth periodic travelling wave.

Table 1: Convergence order in space of **SFP-CH** with a smooth solution.

N	L_1	Order	L_∞	Order
8	3.3401e-03		6.2049e-03	
16	3.3374e-05	6.6450	9.1614e-05	6.0817
32	3.4779e-08	9.9063	1.1768e-07	9.6046
64	1.9335e-08	0.8470	6.3695e-08	0.8856

Table 2: Convergence order in time of **SFP-CH** with a smooth solution.

Δt	L_1	Order	L_∞	Order
a/1000	5.7468e-06		1.1380e-05	
a/2000	1.4294e-06	2.0073	2.8376e-06	2.0038
a/4000	3.5005e-07	2.0298	7.0187e-07	2.0154
a/8000	8.0562e-08	2.1194	1.6819e-07	2.0611

Example 4.2. Single peakon solution for the CH equation

The CH equation (2.1) possess a single peaked travelling wave solution with the initial condition

$$u(x,0)=\begin{cases}\dfrac{c}{\cosh(a/2)}\cosh(x-x_0), & |x-x_0|\le a/2,\\ \dfrac{c}{\cosh(a/2)}\cosh(a-(x-x_0)), & |x-x_0|>a/2,\end{cases} \tag{4.1}$$

where a represents the wave period and c is the wave velocity. In this example, we set the parameters as $a=1$, $c=1$ and $x_0=0$. We also test the convergence order for scheme **SFP-CH** at time $t=1$. For this non-smooth solution, we cannot expect the spectral convergence. However, from Table 3, the scheme converges nevertheless with only first-order accuracy which shares the similar result with [11,23]. Even though scheme **SFP-CH** suffers the order reduction, for a fixed space grid N, the corresponding error is small enough to guarantee the correct long-time simulations which can be verified from the wave profile at $t=50$ in Fig. 2.

Table 3: Convergence order in space of **SFP-CH** with initial condition (4.1).

N	L_1	Order	L_∞	Order
16	1.5345e-03		5.6187e-03	
32	5.9302e-04	1.3716	3.0881e-03	0.8635
64	2.6030e-04	1.1879	1.6272e-03	0.9243
128	1.2394e-04	1.0705	8.5787e-04	0.9236

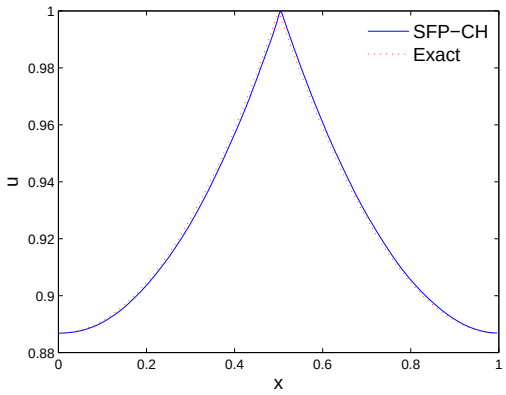

Figure 2: Peakon profile at $t=50$ by scheme **SFP-CH**.

Example 4.3. Multipeakon interaction for the CH equation

The CH equation admits the multipeakon solutions with the initial condition

$$u(x,0)=\sum_{i=1}^{M}\phi_i(x), \tag{4.2}$$

where

$$\phi_i(x)=\begin{cases}\dfrac{c_i}{\cosh(a/2)}\cosh(x-x_i), & |x-x_i|\le a/2,\\ \dfrac{c_i}{\cosh(a/2)}\cosh(a-(x-x_i)), & |x-x_i|>a/2,\quad i=1,2,\cdots,M.\end{cases}\tag{4.3}$$

Here, M denotes the number of peakons. In this example, we investigate the interactions of two and three peakons by setting $M=2$ and 3. For the two-peakon interaction, the parameters are taken as $c_1=2$, $c_2=1$, $x_1=-5$, $x_2=5$, $a=50$. For the three-peakon in-

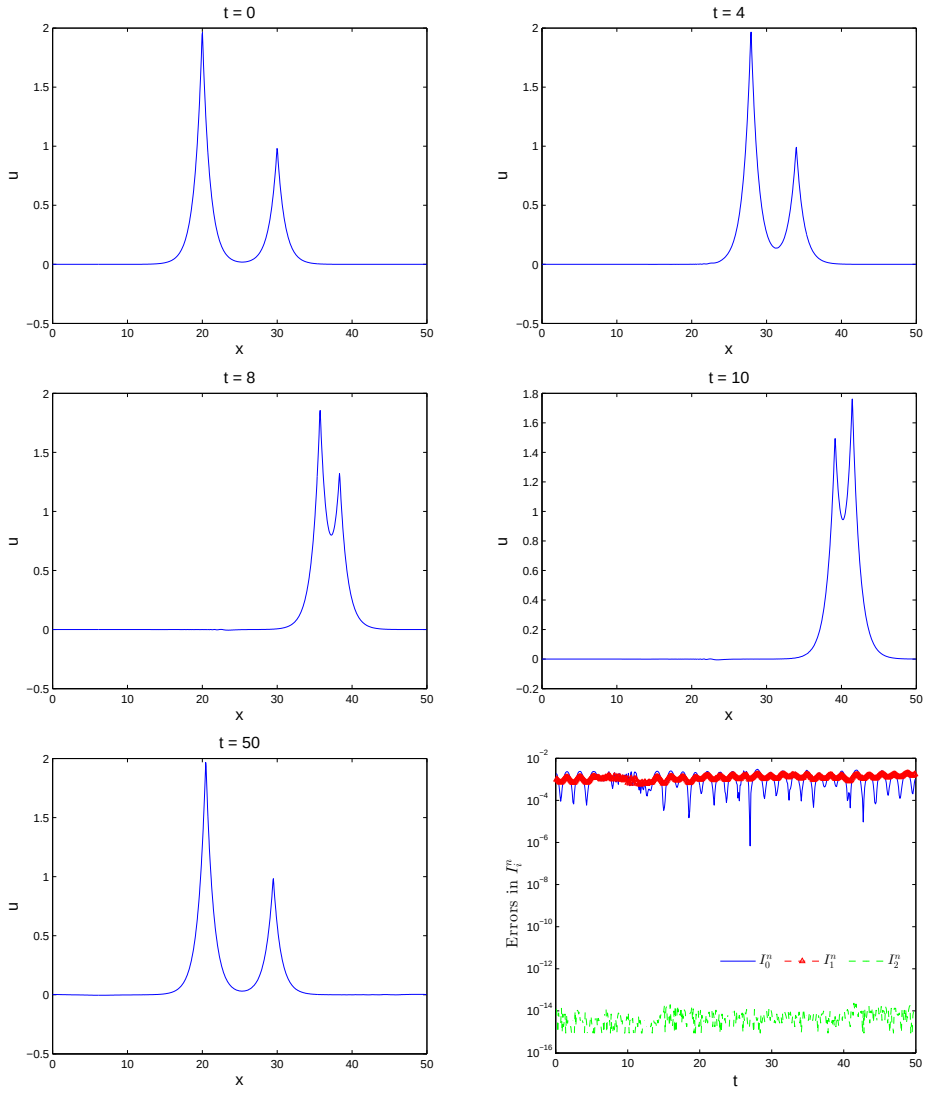

Figure 3: Two-peakon interaction waveforms of the CH equation at different times by **SFP-CH** with $\Delta x=50/1024$, $\Delta t=0.001$ and the errors in three invariants.

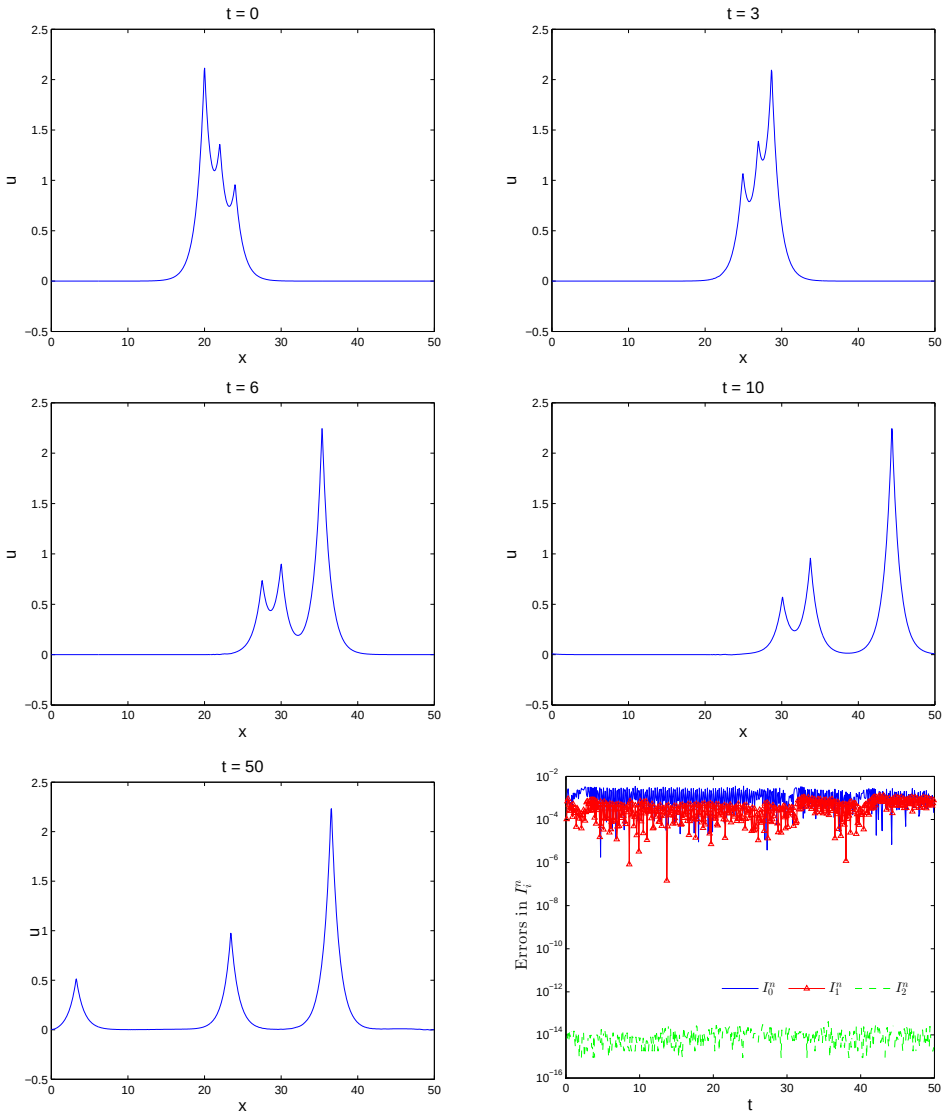

Figure 4: Three-peakon interaction waveforms of the CH equation at different times by **SFP-CH** with $\Delta x = 50/1024$, $\Delta t = 0.001$ and the errors in three invariants.

teraction, the parameters are taken as $c_1 = 2$, $c_2 = 1$, $c_3 = 0.8$, $x_1 = -5$, $x_2 = -3$, $x_3 = -1$, $a = 50$. The simulation is produced by scheme **SFP-CH**, and the computation domain is $[0,a]$. Figs. 3-4 present the snapshots of the peakon wave profiles at different times. From the time domain $[0,10]$, we can see the interactions of both two and three peakon waves are simulated very clearly. Moreover, the wave profiles at $t = 50$ are also well resolved without any spurious waves. For the two cases, errors in invariants I_0^n, I_1^n are bounded while the error in I_2^n is preserved to the machine precision over a long-time interval.

In the following examples, we simulate several kinds of solutions of the DP equation by using schemes **SFP-DP** and **OSM-DP**. It should be noticed that scheme **SFP-DP** is a symplectic integrator which can simulate well the peakon and multipeakon solutions, but fails to simulate the discontinuous shockpeakon wave while scheme **OSM-DP** can handle both the peakon and shockpeakon cases.

Example 4.4. Single peakon

The DP equation (2.2) has a single peaked traveling wave solution which is

$$u(x,t)=ce^{-|x-ct|}, \tag{4.4}$$

where c expresses the wave speed which is chosen as $c=0.25$ in our computation. Since the single soliton decays exponentially when x approaches to $\pm\infty$, we can compute the Cauchy problem of the DP equation in a finite spatial domain with periodic boundary condition. Here, we take the computation domain as $[-20,20]$.

As pointed in [40], when using the pseudo-spectral method to make a global approximation for a non-smooth function, only first-order convergence can be obtained away from the discontinuities and $\mathcal{O}(1)$ spurious Gibbs oscillations are exhibited at the discontinuities. Similar as Example 4.2 about scheme **SFP-CH** for the CH equation, we cannot expect the spectral convergence of scheme **SFP-DP** for the DP equation either, even away from the peakon. However, for a fixed grid number N, scheme **SFP-DP** again possesses very small errors which is demonstrated in Fig. 5 with the amplitude 10^{-5} during a large time interval $[0,50]$.

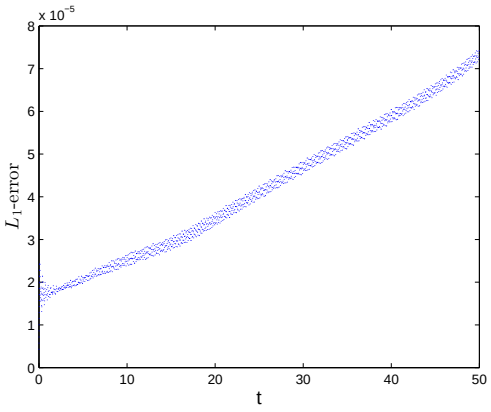

Figure 5: The L_1-errors of numerical solutions in $t\in[0,50]$, with $\Delta x=40/1024$ and $\Delta t=0.01$ by **SFP-DP**.

Furthermore, since we have two numerical schemes for the DP equation, we thereafter make a comparison from the simulation of the single peakon. Firstly, we present the point-wise error at $t=1$ for schemes **SFP-DP** and **OSM-DP** respectively in Fig. 6. It is easy to observe that scheme **SFP-DP** has the oscillations near the peakon even we use a finer mesh which is exactly caused by the Gibbs phenomenon because the derivative of

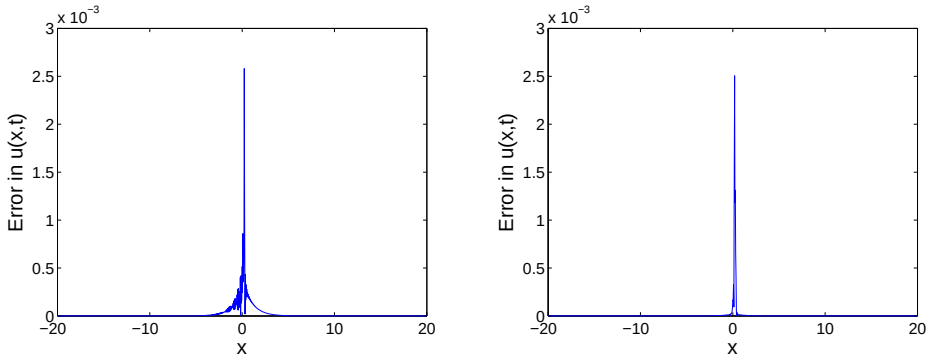

Figure 6: Errors of numerical solutions at $t=1$, with $\Delta x=40/1024$ and $\Delta t=0.01$ by **SFP-DP** (left) and **OSM-DP** (right).

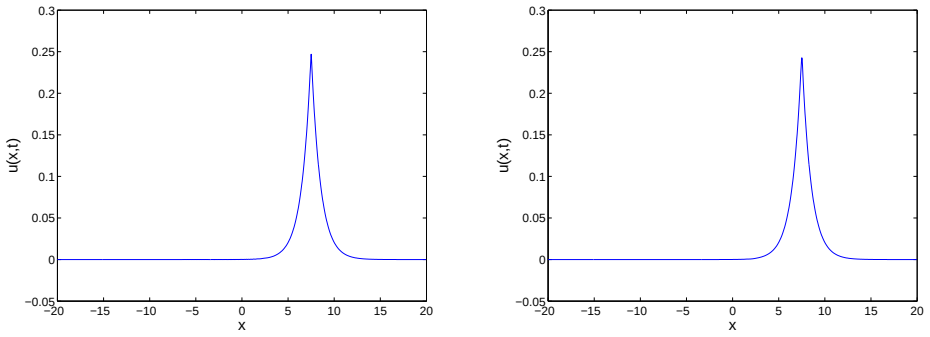

Figure 7: Numerical solutions at $t=30$ with $\Delta x=40/1024$, $\Delta t=0.01$ by **SFP-DP** (left) and **OSM-DP** (right).

the solution is not smooth at the peakon position. While the oscillations can be well resolved by scheme **OSM-DP**. However, the magnitudes of errors do not show a significant difference and the L_∞-norms for both two schemes are nearly the same.

For the long-time numerical behaviour, we present a test on the time interval $[0,30]$. Fig. 7 shows the snapshots of the evolution of the soliton wave at $t=30$. Clearly, there is no spurious wave appeared in the wave propagation for both two schemes. Moreover, we also investigate errors of conserved quantities corresponding to these schemes. From Fig. 8, we noticed that scheme **SFP-DP** can preserve the invariants $\widehat{I}_1^n$ and $\widehat{I}_2^n$ to machine precision while the error in the invariant I_0^n is bounded over the time interval. This verifies the theoretical results obtained above. For scheme **OSM-DP**, it is noticed that the errors in all three invariants have a slightly linear growth. This indicates that scheme **OSM-DP** can not preserve any of three invariants exactly even for a linear one.

The computing time for schemes **SFP-DP** and **OSM-DP** is shown in Table 4. As scheme **SFP-DP** is the pseudo-spectral method, the FFT algorithm can be used. This reduces dramatically the computational cost. Although in the implementation of scheme **OSM-DP**, we also apply the FFT algorithm, the total cost is still very expensive because of the involvement of splitting and composition process.

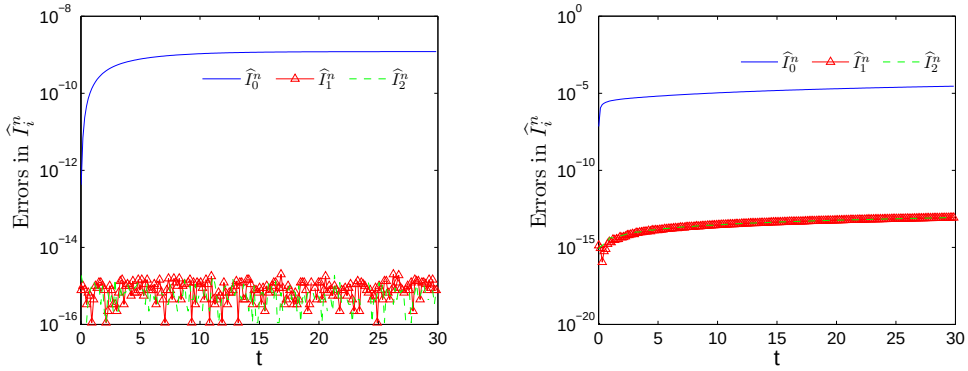

Figure 8: Numerical errors in three invariants with $\Delta x = 40/1024$, $\Delta t = 0.01$ by **SFP-DP** (left) and **OSM-DP** (right).

Table 4: CPU time for single peakon solution with different grid sizes over $[0,30]$.

Δx	40/512	40/1024	40/2048
SFP-DP	1.2687s	2.4804s	5.4814s
OSM-DP	76.5092s	132.4078s	250.5352s

The above comparisons suggest that scheme **SFP-DP** is superior to scheme **OSM-DP** in simulating the peakon solutions. Thus, in Example 4.5 we only apply scheme **SFP-DP** to do the computation.

Example 4.5. Two-peakon interaction

We simulate the behavior of two-peakon interaction for the DP equation by taking the initial condition

$$u_0(x) = m_1 e^{-|x-x_1|} + m_2 e^{-|x-x_2|}, \tag{4.5}$$

where $m_1 = 2, m_2 = 1$ and $x_1 = -13.792, x_2 = -4$. In fact, the analytic expression of the general n-peakon solution has been constructed by Lundmark in [27]. When $n = 2$, the 2-peakon solution is

$$u(x,t) = m_1(t) e^{-|x-x_1(t)|} + m_2 e^{-|x-x_2(t)|},$$

where

$$x_1(t) = \log \frac{(\lambda_1-\lambda_2)^2 b_1 b_2}{(\lambda_1+\lambda_2)(\lambda_1 b_1 + \lambda_2 b_2)}, \quad x_2(t) = \log(b_1+b_2),$$
$$m_1(t) = \frac{(\lambda_1 b_1 + \lambda_2 b_2)^2}{\lambda_1\lambda_2(\lambda_1 b_1^2 + \lambda_2 b_2^2 + \frac{4\lambda_1\lambda_2}{\lambda_1+\lambda_2} b_1 b_2)}, \quad m_2(t) = \frac{(b_1+b_2)^2}{\lambda_1 b_1^2 + \lambda_2 b_2^2 + \frac{4\lambda_1\lambda_2}{\lambda_1+\lambda_2} b_1 b_2},$$

with $b_k(t) = b_k(0) e^{t/\lambda_k}$ satisfying $b_1 + b_2 = e^{x_2}$ and $\frac{b_1}{\lambda_1} + \frac{b_2}{\lambda_2} = m_1 e^{x_1} + m_2 e^{x_2}$. Here, λ_1 and λ_2 $(\lambda_1 < \lambda_2)$ are two real nonzero roots of polynomial $1 - (m_1+m_2)z + m_1 m_2 (1 - e^{x_1}/e^{x_2}) z^2$.

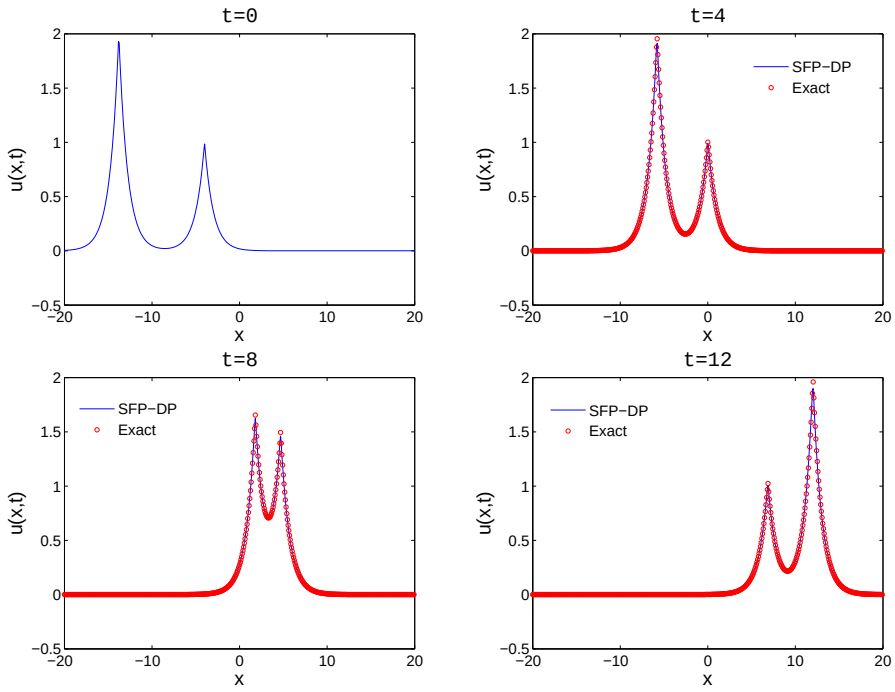

Figure 9: Snapshots of two-peakon interaction of the DP equation at different times by **SFP-DP**.

We use scheme **SFP-DP** to compute the two-peakon solution defined on $[-20,20]$ with periodic boundary condition. Fig. 9 illustrates the snapshots of numerical solutions at $t=0,4,8,12$. It is observed that the interaction of two peakon waves is resolved very well by scheme **SFP-DP**. Fig. 10 shows the numerical errors in three invariants, which implies that scheme **SFP-DP** can preserve invariants $\widehat{I}_1^n$ and $\widehat{I}_2^n$ very well, and can bound the invariant $\widehat{I}_0^n$.

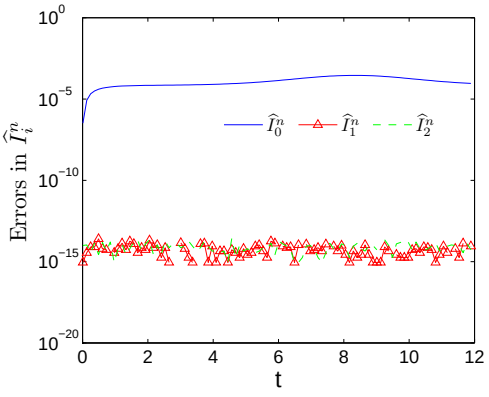

Figure 10: Numerical errors in three invariants with initial condition (4.5) by **SFP-DP**.

Example 4.6. Soliton solution

The DP equation can also admit the multi-soliton solutions which are constructed recently in [30, 31] when $\kappa \neq 0$. In this case, the bi-Hamiltonian structures are not available, so does the corresponding symplectic integrator **SFP-DP**. Here, we use the operator splitting scheme **OSM-DP** to simulate the one soliton solution. The one soliton solution is expressed explicitly as

$$u(x,t) = \frac{8\kappa^3}{a_1} \frac{(a_1^2-1)(a_1^2-\frac{1}{4})}{\cosh\xi_1 + 2a_1 - \frac{1}{a_1}},$$

where ξ_1 satisfies $x - c_1 t - x_{10} = \frac{\xi_1}{\kappa k_1} - \ln\left(\frac{\alpha_1 - 1 + (\alpha_1+1)e^{\xi_1}}{\alpha_1 + 1 + (\alpha_1 - 1)e^{\xi_1}}\right)$ and can be solved by Newton iteration, α_1, a_1, c_1 and x_{10} are constant which are defined by

$$\alpha_1 = \sqrt{\frac{(2a_1-1)(a_1+1)}{(2a_1+1)(a_1-1)}}, \quad a_1 = \sqrt{\frac{1-\frac{1}{4}\kappa^2 k_1^2}{1-\kappa^2 k_1^2}}, \quad c_1 = \frac{3\kappa^3}{1-\kappa^2 k_1^2}, \quad x_{10} = \frac{y_{10}}{\kappa}.$$

We choose $\kappa = 0.511$, $\kappa k_1 = 0.8$, $y_{10} = 0$. Fig. 11 illustrates the exact solution and the numerical solution at $t = 10$ computed by scheme **OSM-DP** with $\Delta t = \Delta x = 40/256$. We can see clearly that although we take a coarse mesh, the performance of the numerical solution is also very good due to the high accuracy of scheme **OSM-DP**. The errors and convergence order at $t=1$ by using the uniform meshes of N cells are listed in Table 5. For this smooth solution, we can both expect the WENO scheme for the Burger's equation and the pseudo-spectral method for the BBM equation to achieve fifth-order as well as infinite-order accuracy in the spatial discretizations. Therefore, the numerical errors are dominated by the WENO scheme and therefore the L_1 and L_∞ errors in Table 5 are supposed to be fifth-order reduction. However, since the analytical solution does not have

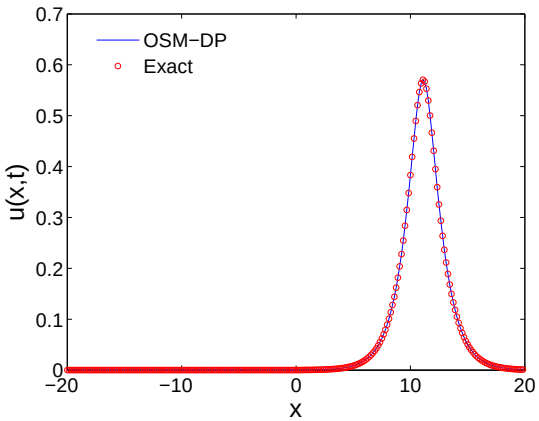

Figure 11: Comparison of the numerical solution by **OSM-DP** and exact solution at $t = 10$.

Table 5: Convergence order of **OSM-DP** in space.

N	L_1	Order	L_∞	Order
64	3.0207e-02		1.2343e-02	
128	3.1855e-03	3.2453	1.6419e-03	2.9102
256	1.8704e-04	4.0901	1.2189e-04	3.7517
512	7.2413e-06	4.6910	6.8972e-06	4.1434
1024	2.4916e-07	4.8611	2.6367e-07	4.7092

a closed form and is approximately obtained by the Newton iteration, the convergence rate can hardly reach the expected order. But we can see the convergence tendency very clearly.

Example 4.7. Wave breaking

For some certain initial profiles, it is known that the DP equation also has the blow-up phenomena which theoretical results have been established in [26]. To perform the blow-up phenomena, we choose the following initial condition

$$u_0(x)=\mathrm{sech}^2(d(x-x_0)), \tag{4.6}$$

where d is a parameter which expresses the width of the initial profile. With this initial condition, the momentum density can be calculated as

$$m_0(x)=u_0(x)-u_{0,xx}(x)=\mathrm{sech}^2(d(x-x_0))\Big(1-4d^2+6d^2\mathrm{sech}^2(d(x-x_0))\Big). \tag{4.7}$$

By the sign of $m_0(x)$, we can determine when the wave breaking may happen. From (4.7), it is noticed that $m_0(x)>0$ if $d<\frac{1}{2}$, and the sign of $m_0(x)$ may change when $d>\frac{1}{2}$. To confirm further, we take two initial values in the form of (4.6) with $x_0=-20$, $d=0.3$ and d=2, respectively. Since the shock waves usually appear after wave breaking, we here use scheme **OSM-DP** to simulate the case of $d=2$ and scheme **SFP-DP** to simulate the case of $d=0.3$. Fig. 12 and Fig. 13 show the numerical solutions and errors in three invariants when d is taken as $d=0.3$ and $d=2$, respectively. We take the space step $\Delta x=80/1024$ and the time step $\Delta t=0.01$. It is shown that in Fig. 13 the magnitude of the error in $\widehat{I}_2^n$ is still very small, but the invariant $\widehat{I}_0^n$ is no longer conserved. This is consistent with the theoretical results presented in [27]. Another example of the wave breaking phenomenon is provided in [8,16] with the initial condition

$$u_0(x)=e^{0.5x^2}\sin(\pi x). \tag{4.8}$$

The computation domain is taken as $[-2,2]$. We use $N=512$ be the number of grid points and $\Delta t=0.001$. In Fig. 14, the shock peakon profiles at $t=0$, 0.12, 0.18, 0.3, 0.5 and 1.1 are shown. In Fig. 15, it is shown that the invariant $\widehat{I}_2^n$ can be preserved up to round-off error.

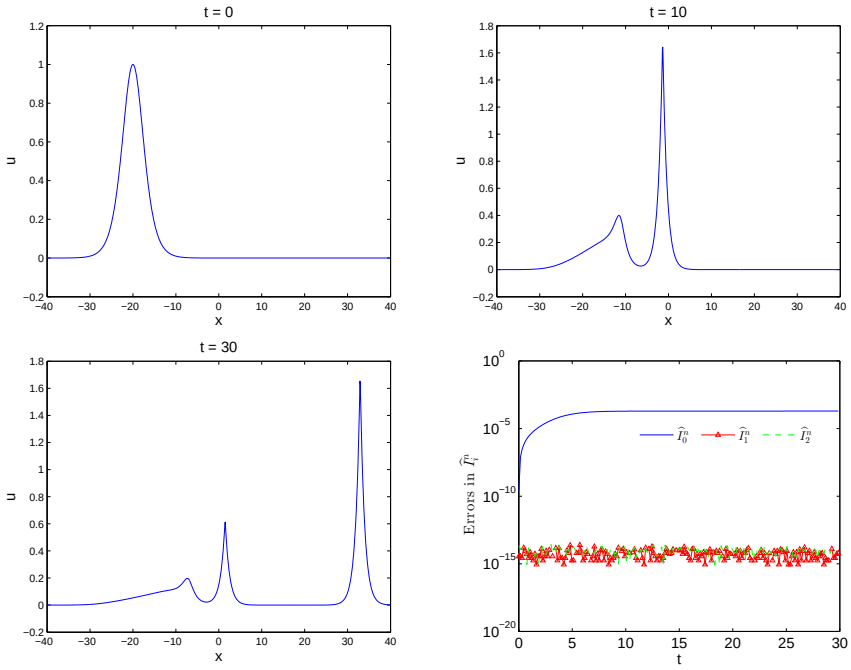

Figure 12: Snapshots for the initial condition (4.6) with $d=0.3$ computed by **SFP-DP** and errors in three invariants.

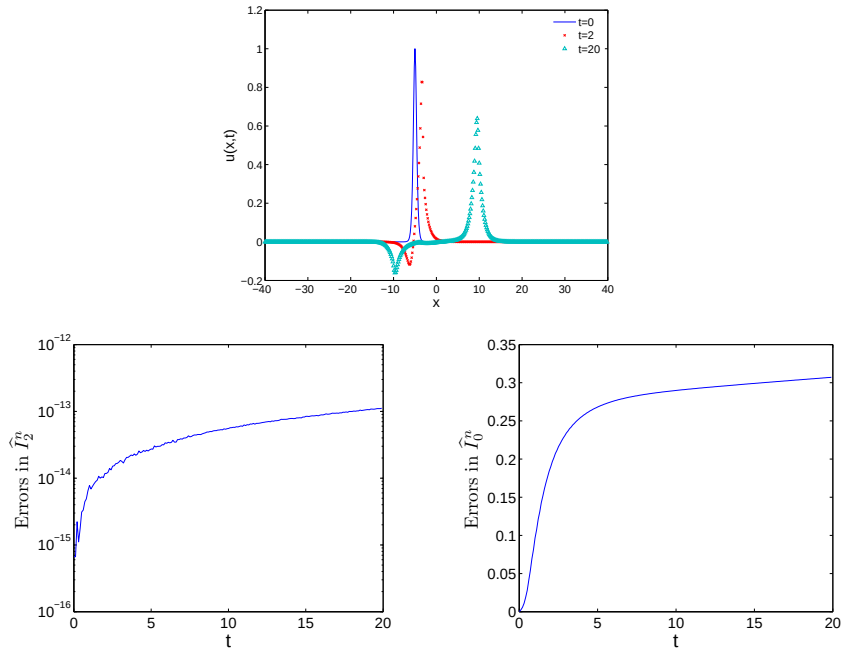

Figure 13: The case of $d=2$ computed by **OSM-DP**. Numerical solutions at $t=0,2,20$ (top); Error in invariant $\widehat{I}_2^n$ (left bottom); Error in invariant $\widehat{I}_0^n$ (right bottom).

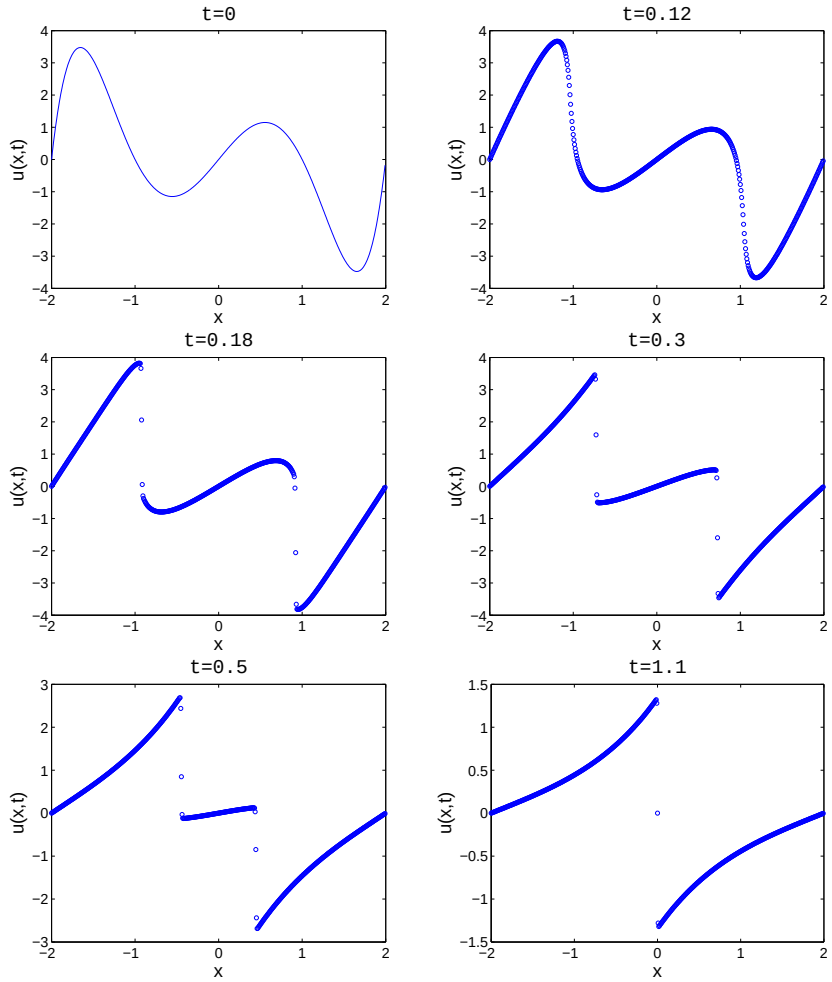

Figure 14: Shock formation of the DP equation by **OSM-DP** at different time with initial condition (4.8).

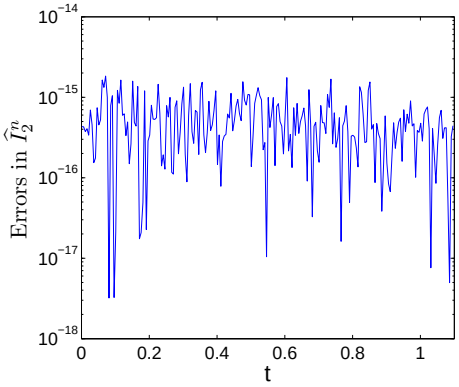

Figure 15: Error in invariant $\widehat{I}_2^n$ by **OSM-DP** with the initial condition (4.8).

Example 4.8. Peakon-antipeakon interaction

Lundmark [27] has studied in detail the solutions involving peakons and antipeakons, and showed when a peakon collides with an antipeakon the jump discontinuity which is often called "shockpeakon", will appear. As follows, we will confirm numerically this theoretical results for both the symmetric $(m_1+m_2)=0$ case and nonsymmetric $(m_1+m_2)\neq 0$ cases with m_1,m_2 the coefficients in (4.5). As the solution is not very smooth, we simulate the wave by using scheme **OSM-DP**.

For the symmetric case, we choose the initial condition in form of (4.5) with $m_1=1, m_2=-1, x_1=-5$ and $x_2=5$. Before collision, the solution is a two-peakon wave. At $t_c\approx 5$ the collision happens, this produces a stationary shock decaying shockpeakon wave.

For the nonsymmetric case, we choose the initial values in form of (4.5) with $m_1=2$, $m_2=-1$, $x_1=-5$ and $x_2=5$. The collision occurs at $t_c\approx 3.3628$. After collision, there appears a shockpeakon wave which moves to the right as the peakon wave is stronger than the antipeakon wave in amplitude.

Fig. 16 and Fig. 17 show the numerical solutions and the exact solution at different time for the symmetric and nonsymmetric cases. The numerical results show that the numerical solution and the exact solution are excellently matched, even the numerical solution can catch the collision very well. We also illustrate the numerical errors of invariant $\widehat{I}_2^n$ for both cases in Fig. 18. The numerical result states that $\widehat{I}_2^n$ can be preserved

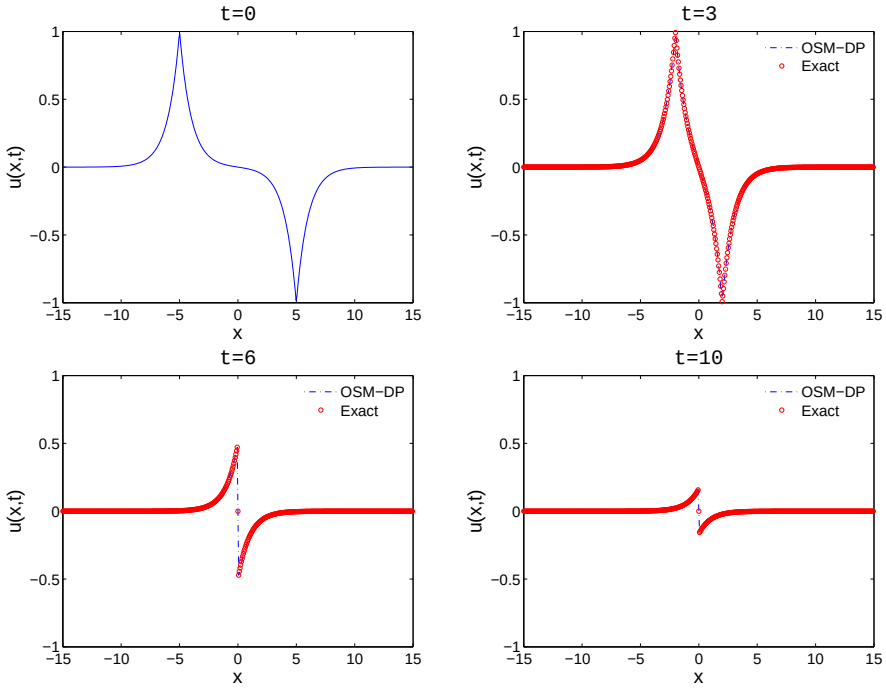

Figure 16: Peakon-antipeakon interaction in the symmetric case by **OSM-DP** with $\Delta x=30/1024, \Delta t=0.01$ at different times.

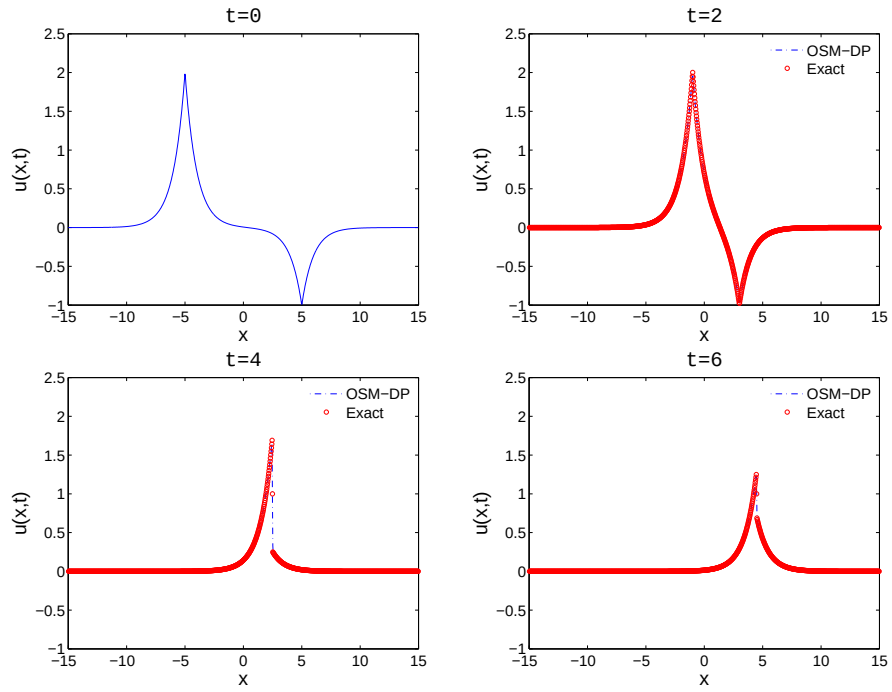

Figure 17: Peakon-antipeakon interaction in the nonsymmetric case by **OSM-DP** with $\Delta x=30/1024$, $\Delta t=0.01$ at different times.

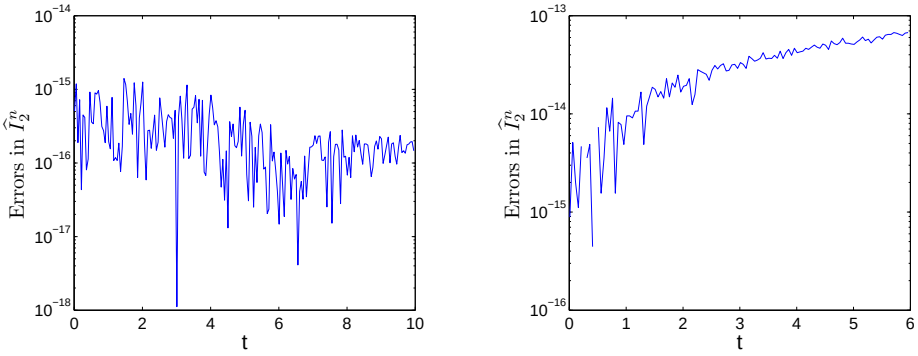

Figure 18: Error in $\widehat{I}_2^n$ for peakon-antipeakon interaction by **OSM-DP** for symmetric case (left) and nonsymmetric case (right).

by scheme **OSM-DP** for the symmetric solution while for the nonsymmetric case, the numerical error in $\widehat{I}_2^n$ grows linearly with very small range.

Example 4.9. Shockpeakon-shockpeakon interaction

As the DP equation can admit a shockpeakon wave, we can also investigate the interaction of two shock peakon waves. We adopt the following initial condition introduced

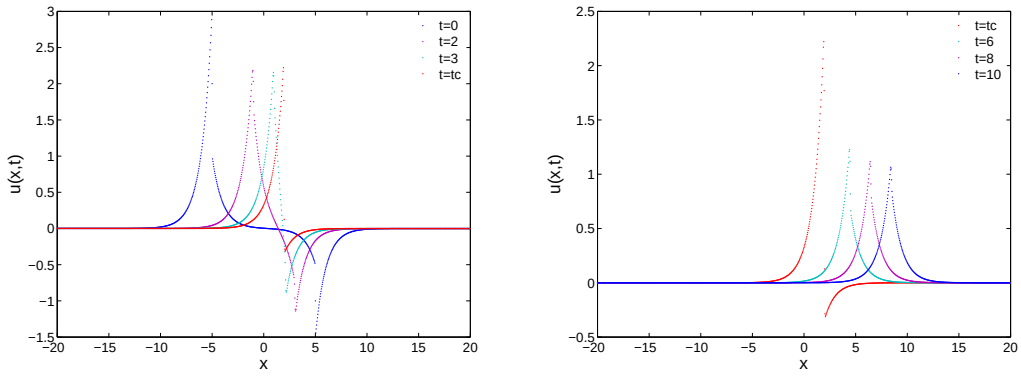

Figure 19: Shockpeakon-shockpeakon interaction by **OSM-DP** before collision (left) and after collision (right).

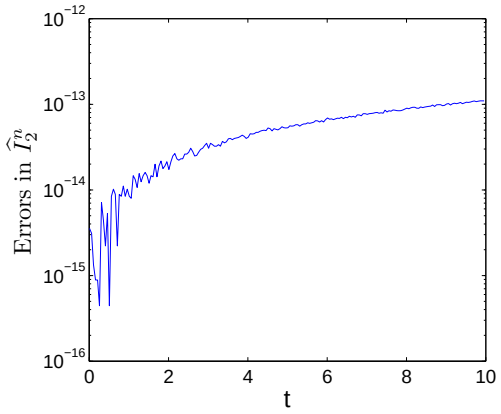

Figure 20: Error in $\widehat{I}_2^n$ by **OSM-DP** with the initial condition (4.9).

in [16]

$$u_0(x)=2e^{-|x+5|}-\mathrm{sgn}(x+5)\mathrm{e}^{-|x+5|}-\mathrm{e}^{-|x-5|}-0.5\mathrm{sgn}(x-5)\mathrm{e}^{-|x-5|}. \tag{4.9}$$

The evolutionary behavior of two shock peakon waves is plotted in Fig. 19. It is clear that the initial wave (4.9) is a two shockpeakon wave, which will merge into a single shockpeakon wave at $t_c \approx 3.5$. The global error of conserved quantity $\widehat{I}_2^n$ is plotted in Fig. 20 which shows a linear growth even though the error is not very large.

From the above experiments, it is observed that for the problems with symmetric solutions, such as the wave breaking phenomena with initial condition (4.8), the symmetric peakon-antipeakon interaction, scheme **OSM-DP** can conserve the invariant $\widehat{I}_2^n$ up to round-off error. But for the nonsymmetric cases, the error of invariant $\widehat{I}_2^n$ increases linearly with very small amplitude.

5 Concluding remarks

We have simulated the solutions of the CH and DP equations with different initial values by using two symplectic integrators: **SFP-CH** and **SFP-DP**, and one operator splitting method **OSM-DP**. The two symplectic schemes are actually the pseudo-spectral methods constructed based on Hamiltonian formulations of the CH equation and the DP equation, respectively. It has been analyzed that the DP equation can be split into the Burgers' equation and the BBM equation, by combining the WENO scheme for the Burgers' equation and the multisymplectic pseudo-spectral method for the BBM equation we have constructed scheme **OSM-DP**. For the DP equation, we have given the comprehensive numerical tests and comparisons by using schemes **SFP-DP** and **OSM-DP** which show that scheme **SFP-DP** is outstanding in simulating the peakon solutions because of its less computation cost with the use of the fast Fourier transform and superior conservative properties, but it fails in tracking the shock wave solution. It is also shown that scheme **OSM-DP** has the better ability to simulate the smooth soliton solution and shock wave solutions. To simulate the peakon solutions, we can use scheme **OSM-DP**, but its computation cost is a little high.

Acknowledgments

This research was supported by the National Natural Science Foundation of China 11271357, 11271195 and 41504078, by the CSC, the Foundation for Innovative Research Groups of the NNSFC 11321061 and the ITER-China Program 2014GB124005.

References

[1] R. Beals, D.H. Sattinger, and J. Szmigielski. Multi-peakons and a theorem of Stieltjes. *Inv. Prob.*, 15:L1–L4, 1999.
[2] R. Beals, D.H. Sattinger, and J. Szmigielski. Multipeakons and the classical moment problem. *Adv. Math.*, 154:229–257, 2000.
[3] T.B. Benjamin, J.L. Bona, and J. Mahony. Model equations for long waves in nonlinear dispersive systems. *Phil. R. Soc.*, 272:47–78, 1972.
[4] T.J. Bridges and S. Reich. Multi-symplectic spectral discretizations for the Zakharov-Kuznetsov and shallow water equations. *Physica D*, 152-153:491–504, 2001.
[5] R. Camassa and D.D. Holm. A integrable shallow water equation with peaked solutions. *Phys. Rev. Lett.*, 71:1661–1664, 1993.
[6] R. Camassa, D.D. Holm, and J.M. Hyman. A new integrable shallow water equation. *Adv. Appl. Mech.*, 31:1–33, 1994.
[7] J.B. Chen and M.Z. Qin. Multi-symplectic Fourier pseudospectral method for the nonlinear Schrödinger equation. *Electon. Trans. Numer. Anal.*, 12:193–204, 2001.
[8] G.M. Coclite, K. Karlsen, and N. Risebro. Numerical schemes for computing discontinuous solutions of the Degasperis-Procesi equation. *IMA J. Numer. Anal.*, 28:80–105, 2008.

[9] G.M. Coclite and K.H. Karlsen. On the well-posedness of the Degasperis-Procesi equation. *J. Funct. Anal.*, 233:60–91, 2006.
[10] G.M. Coclite and K.H. Karlsen. On the uniqueness of discontinuous solutions to the Degasperis-Procesi equation. *J. Differ. Equations*, 234:142–160, 2007.
[11] D. Cohen, B. Owren, and X. Raynaud. Multi-symplectic integration of the Camassa-Holm equation. *J. Comput. Phys.*, 227:5492–5512, 2008.
[12] A. Constantin and D. Lannes. The hydrodynamical relevance of the Camassa-Holm and Degasperis-Procesi equation. *Arch. Ration. Mech. Anal.*, 192:165–186, 2009.
[13] A. Degasperis, D.D. Holm, and A.H.W. Hone. A new integrable equation with peakon solutions. *Theor. Math. Phys.*, 133:1463–1474, 2002.
[14] A. Degasperis and M. Procesi. Asymptotic integrability. In *Symmetry and Perturbation Theory*, pages 22–37. World Scientific Publishing, 1999.
[15] J. Escher, Y. Liu, and Z. Yin. Global weak solutions and blow-up structure for the Degasperis-Procesi equation. *J. Funct. Anal.*, 241:457–485, 2006.
[16] B. Feng and Y. Liu. An operator splitting method for the Degasperis-Procesi equation. *J. Comput. Phys.*, 228:7805–7820, 2009.
[17] S. Gottlieb and C.-W. Shu. Total variation diminishing Runge-Kutta schemes. *Math. Comput.*, 67:73–85, 1998.
[18] S. Gottlieb, C.-W. Shu, and E. Tadmor. Strong stability preserving high order time discretization methods. *SIAM Rev.*, 43:89–112, 2001.
[19] E. Hairer, C. Lubich, and G. Wanner. *Geometric Numerical Integration: Structure-Preserving Algorithms for Ordinary Differential Equations*. Springer-Verlag, Berlin, second edition, 2006.
[20] H. Hoel. A numerical scheme using multi-shockpeakons to compute solutions of the Degasperis-Procesi equation. *Electron. J. Differential Equations*, 2007:1–22, 2007.
[21] G. Jiang and C.-W. Shu. Efficient implementation of Weighted ENO schemes. *J. Comput. Phys.*, 126:202–228, 1996.
[22] R.S. Johnson. Camassa-Holm, Korteweg-de Vries and related models for water. *J. Fluid Mech.*, 455:63–82, 2002.
[23] H. Kalisch and J. Lenells. Numerical study of traveling-wave solutions for the Camassa-Holm equation. *Chaos Soliton Fract.*, 25:287–298, 2005.
[24] H. Kalisch and X. Raynaud. Convergence of a spectral projection of the Camassa-Holm equation. *Numer. Meth. Part. D. E.*, 22:1197–1215, 2006.
[25] H. Liu, Y. Huang, and N. Yi. A conservative discontinuous Galerkin method for the Degasperis-Procesi equation. *Methods Appl. Anal.*, 21:83–106, 2014.
[26] Y. Liu and Z. Yin. Global existence and blow-up phenomena for the Degasperis-Procesi equation. *Comm. Math. Phys.*, 267:801–820, 2006.
[27] H. Lundmark. Formation and dynamics of shock waves in the Degasperis-Procesi equation. *J. Nonlinear. Sci.*, 17:169–198, 2007.
[28] H. Lundmark and J. Szmigielski. Degasperis-Procesi peakons and the discrete cubic string. *Int. Math. Res. Pap.*, 2005:53–116, 2003.
[29] H. Lundmark and J. Szmigielski. Multi-peakon solutions of the Degasperis-Procesi equation. *Inv. Prob.*, 19:1241–1245, 2003.
[30] Y. Matsuno. Multisoliton solutions of the Degasperis-Procesi equation. *Inv. Prob.*, 21:2085–2101, 2005.
[31] Y. Matsuno. Multisoliton solutions of the Degasperis-Procesi equation and their peakon limit. *Inv. Prob.*, 21:1553–1570, 2005.
[32] Y. Miyatake and T. Matsuo. Conservative finite difference schemes for the Degasperis-

Procesi equation. *J. Comput. Appl. Math.*, 236:3728–3740, 2012.
[33] P.J. Olver. On the Hamiltonian structure of evolution equations. *Math. Proc. Camb. Phil. Soc.*, 88:71–88, 1980.
[34] J. Shen, T. Tang and L.-L. Wang. *Spectral Methods: Algorithms, Analysis and Applications*. Springer, 2011.
[35] C.-W. Shu. Essentially non-oscillatory and weighted essentially non-oscillatory schemes for hyperbolic conservation laws. In *Advanced Numerical Approximation of Nonlinear Hyperbolic Equations*, pages 325–432. Springer Berlin Heidelberg, 1998.
[36] C.-W. Shu. Total-Variation-Diminishing time discretizations. *SIAM J. Sci. Stat. Comput.*, 9:1073–1084, 1998.
[37] C.-W. Shu and S. Osher. Efficient implementation of essentially non-oscillatory shock-capturing schemes. *J. Comput. Phys.*, 77:439–471, 1998.
[38] Y.J. Sun and M.Z. Qin. A multi-symplectic scheme for RLW equation. *J. Comput. Math.*, 22:611–621, 2004.
[39] L.N. Trefethen. *Spectral Methods in MATLAB*. SIAM, Philadelphia, 2000.
[40] Y. Xia. Fourier spectral methods for Degasperis-Procesi equation with discontinuous solutions. *J. Sci. Comput.*, 61:584–603, 2014.
[41] Y. Xu and C.-W. Shu. Local discontinuous Galerkin methods for the Degasperis-Procesi equation. *Commun. Comput. Phys.*, 10:474–508, 2011.
[42] H. Yoshida. Construction of higher order symplectic integrators. *Phys. Lett. A*, 150:262–268, 1990.
[43] H. Yoshida. Fractal decomposition of exponential operators with applications to many-body theories and Monte Carlo simulations. *Phys. Lett. A*, 146:319–323, 1990.
[44] C.H. Yu and Tony W.H. Sheu. A dispersively accurate compact finite difference method for the Degasperis-Procesi equation. *J. Comput. Phys.*, 236:493–512, 2013.